Quantum three-wave instability

Michael Q. May [*] and Hong Qin [†]
Plasma Physics Laboratory, Princeton University, Princeton, New Jersey 08540, USA

(Received 22 August 2022; accepted 4 May 2023; published 6 June 2023)

For the three-wave interaction, the lowest-order nonlinear interaction in plasma dynamics, we describe how the quantum system, which is time-independent, nonchaotic, finite-dimensional, and Hermitian, can give rise to a linear instability corresponding to that in the classical system. We show that the instability is realized in the quantum regime as a cascade of the wave function in the space of occupation number states, and the unstable quantum system has a richer spectrum and a much longer recurrence time than the stable quantum system. The conditions for instability of the quantum three-wave interaction are described.

DOI: 10.1103/PhysRevA.107.062204

I. INTRODUCTION

The three-wave interaction, the lowest-order nonlinear interaction in plasma dynamics, has applications in laser-plasma interactions [1,2], determining weak turbulence spectra [3], and nonlinear optical system design [4–6]. Classically, the linear dynamics of the interaction are affected by a parametric instability before developing into the nonlinear regime [7]. Physically, this instability is triggered when one large amplitude wave denoted by (ω_1, k_1) resonates with two others, denoted by (ω_2, k_2) and (ω_3, k_3). In the so-called decay interaction the resonance conditions are $\omega_1 = \omega_2 + \omega_3$ and $k_1 = k_2 + k_3$, which ensure energy-momentum conservation. The instability transfers energy-momentum from the large wave to the two smaller waves. Although this interaction and instability are well known [8–11], its quantum description is less studied [7,12–15] and the correspondence between the classical instability and its quantum counterpart has not been established. The three-wave interaction was recently simulated on a quantum computer [14], and although the simulation was not of high-enough dimension to allow for the instability, it will not be long before quantum simulations large enough to simulate the instability are possible.

For classically nonintegrable systems, the fields of quantum chaos and random matrix theory provide a means of characterizing correspondingly unstable quantum behavior (see, for example, Refs. [16,17] on the subject and Refs. [18,19] for earlier work on time-dependent Hamiltonians). However, the classical three-wave system is integrable and can be solved exactly in terms of Jacobi elliptic functions [20]. As will be shown in Sec. II, the dynamics of the classical three-wave interaction are constrained by three conserved quantities. The category of quantum integrability is more complicated and contested (see Ref. [21]), but the quantum system is constrained by an analogous set of three conserved quantities. In addition, as will be shown in Sec. IV B, the spacing of the quantum Hamiltonian's eigenvalues is not Wignerian, as would be expected from a chaotic, random matrix.

There is recent work on quantum instabilities in time-independent, finite Hermitian systems with nonchaotic classical behavior [22–26], much of which focused on the use of out-of-time-order-correlators (OTOCs) to identify both criteria for the onset of chaos and proximity to fixed point dynamics relevant to nonchaotic instability. Unlike much of that work, we determine the existence of the three-wave instability via an analytic calculation of the exponential behavior of a quantum observable when the quantum system is near the classical fixed point, and the quantum observable we investigate directly corresponds to a classical observable. There has also been research into quantum instabilities in plasma physics, but it has been restricted to infinite-dimensional or non-Hermitian systems including PT-symmetric Hamiltonians [27–33] and pseudo-Hermitian Hamiltonians [34]. Additionally, research into nonchaotic quantum instabilities in systems formally similar to the three-wave interaction, including quadratic Hermitian squeezing Hamiltonians [35–37], have also been restricted to infinite-dimensional cases.

In classical-dynamical systems, a linear instability is characterized by the existence of an eigenfrequency with positive imaginary part, i.e., growth rate. This is impossible in a time-independent, finite quantum system since the dynamics are unitary and its eigenfrequencies are real. However, the unitary nature of Hermitian quantum systems does not preclude the exponential growth of an observable that does not commute with the Hamiltonian. In the present study, we define an instability of an observable as a solution of the system for which the expected value of the observable deviates exponentially from the initial condition. When such an instability exists, we say that the quantum system is unstable with respect to the observable.

Section II will focus on providing background to the classical three-wave instability and the quantum theory of three-wave interaction by Shi *et al.* [7,13–15]. In Sec. III, the quantum three-wave interaction equation will be approximately solved in the linear regime and an unstable solution

[*] mqmay@princeton.edu
[†] hongqin@princeton.edu

will be found, demonstrating the existence of a quantum instability according to our definition. This unstable quantum solution will be compared with the classical solution and the classical limit of the quantum instability will be discussed. Numerical results showing the validity of the approximate linear solution of the quantum instability will also be presented. In Sec. IV, we will show how the quantum instability is realized as a cascade of the wave function in the space of the occupation number statues. The expected occupation number of a quantum solution in terms of the eigenvalues of the Hamiltonian will be derived. It shows a richer spectrum in the unstable system than in the stable system. The eigenvalues of the stable Hamiltonian are linearly distributed while the eigenvalues of the unstable Hamiltonian are nonlinearly distributed. Finally, Sec. V concludes with a discussion of the requirements for realizing the quantum instability on quantum hardware.

II. THREE-WAVE INTERACTION

In an ordinary gas, sound waves may nonlinearly self-steepen due to interactions between the principle wave and its higher-frequency resonances. This is possible because each of the wave frequencies is a normal mode of the system and therefore allowed. By contrast, most plasmas' dispersion relations are very dispersive, so nonlinear interactions of a single wave with its higher-frequency resonances are negligible. The lowest-order nonlinear interaction in plasma dynamics is thus the three-wave interaction, where a single wave interacts resonantly with two others. For example, two Alfvén waves can interact nonlinearly with a sound wave in a homogeneous plasma [38].

A. Classical theory for three-wave interaction and instability

In the classical theory, the nonlinear dynamics of the homogeneous three-wave interaction may be reduced to [10,11,39,40]

$$\partial_t A_1 = g A_2 A_3, \tag{1}$$

$$\partial_t A_2 = -g^* A_1 A_3^*, \tag{2}$$

$$\partial_t A_3 = -g^* A_1 A_2^*, \tag{3}$$

where g is a coupling coefficient, A_j is the amplitude of the jth wave, and A_j^* its complex conjugate. Equations (1) to (3) are the canonical Hamilton's equations corresponding to the Hamiltonian

$$H = g A_1^* A_2 A_3 - g^* A_1 A_2^* A_3^*, \tag{4}$$

for the the canonical pairs of A_j and A_j^*. By choosing an appropriate normalization, we can let $g = 1$ without losing generality. The governing equations for the wave action $I_j = |A_j|^2$ are found to be

$$\partial_t I_1 = -\partial_t I_2 = -\partial_t I_3 = g A_1^* A_2 A_3 + g^* A_1 A_2^* A_3^*. \tag{5}$$

These obviate two constants of motion in the system

$$s_2 = I_1 + I_3, \tag{6}$$

$$s_3 = I_1 + I_2, \tag{7}$$

so that the growth of the second or third waves will reduce the amplitude of the first. Using these constants of motion while taking another time derivative of Eq. (5), we arrive at closed equations for the classical wave actions

$$\partial_t^2 I_1 = 2\big[s_2 s_3 + 3I_1^2 - 2(s_2 + s_3) I_1\big], \tag{8}$$

$$\partial_t^2 I_2 = 2\big[s_3(s_2 - s_3) - 3I_2^2 + 2(2s_3 - s_2) I_2\big], \tag{9}$$

$$\partial_t^2 I_3 = 2\big[s_2(s_3 - s_2) - 3I_3^2 + 2(2s_2 - s_3) I_3\big]. \tag{10}$$

Note that Eq. (5) implies that the right-hand sides of Eqs. (8) to (10) are equivalent up to a sign change. Equations (8) to (10) are second-order nonlinear differential equations, which may be solved in terms of elliptic integrals and in the special case that $I_2 = I_3$ the solutions for I_1, I_2, and I_3 take on particularly simple forms in terms of the hyperbolic tangent and secant, respectively.

The linear instability of the three-wave system can be equivalently described using Eqs. (1) to (3) or Eqs. (8) to (10). For easy comparison with the quantum result in the next section, we analyze the classical three-wave instability using Eqs. (8) to (10).

In classical theory, linear instability refers to the exponential growth of a deviation relative to an equilibrium solution of a system. For the system studied here, the equilibrium solution of Eqs. (8) to (10) is $I_{10} = \text{cont.} \neq 0$ and $I_{20} = I_{30} = 0$. Consider a perturbation of the system of the form

$$I_1 = I_{10} + \delta I_1\,, \tag{11}$$

$$I_2 = \delta I_2, \tag{12}$$

$$I_2 = \delta I_3. \tag{13}$$

The linearized system for δI_1, δI_2, and δI_3 is

$$\partial_t^2 \delta I_1 = 0\,, \tag{14}$$

$$\partial_t^2 \delta I_2 = 4 I_{10} \delta I_2\,, \tag{15}$$

$$\partial_t^2 \delta I_3 = 4 I_{10} \delta I_3\,. \tag{16}$$

Thus, the system is unstable with growth rate $\gamma = 2\sqrt{I_{10}}$. However, only δI_2 and δI_3 grow exponentially with time. Equations (1) and (14) indicate that, for the unstable eigenmode of the linearized system, δI_1 and δA_1 remain constant.

As will be shown in Sec. III, an equilibrium solution for the quantum system cannot be meaningfully defined. Therefore, for comparison with the quantum solution, we derive the linear dynamics of Eqs. (8) to (10) relative to an initial condition $I_j(0) = I_{ji} \neq 0$ $(j = 1, 2, 3)$. For exact solutions, s_2 and s_3 are conserved, so a solution for I_1 will determine the solutions for I_2 and I_3. Assuming an initial condition and a small deviation of the form

$$I_j = I_{ji} + \delta I_j, \quad (j = 1, 2, 3), \tag{17}$$

Eq. (8) can be rewritten as

$$\partial_t^2 \delta I_1 = 2\{\delta I_1[2(I_{1i} - I_{2i} - I_{3i}) + 3\delta I_1] + I_{2i}I_{3i} - I_{1i}(I_{2i} + I_{3i})\}. \quad (18)$$

Assuming that $\delta I_1 \ll \frac{2}{3}(I_{1i} - I_{2i} - I_{3i})$, which will be true for short times, we may ignore the term proportional to δI_1^2,

$$\partial_t^2 \delta I_1 = 2[\delta I_1 2(I_{1i} - I_{2i} - I_{3i}) + I_{2i}I_{3i} - I_{1i}(I_{2i} + I_{3i})]. \quad (19)$$

Its solution is

$$\delta I_1 = \frac{B_C}{\gamma_C^2} + C_1 e^{\gamma_C t} - \left(\frac{B_C}{\gamma_C^2} + C_1\right) e^{-\gamma_C t}, \quad (20)$$

where

$$\gamma_C = 2\sqrt{I_{1i} - I_{2i} - I_{3i}}, \quad (21)$$

$$B_C = 2I_{1i}(I_{2i} + I_{3i}) - 2I_{2i}I_{3i}. \quad (22)$$

The classical constants γ_C and B_C are written with a subscript "C" to distinguish them from quantum constants γ_Q and B_Q, which will be derived in the next section. The third constant C_1 cannot be determined from the action equations, Eq. (19) and its counterparts for I_2 and I_3, because they each only involve even time derivatives at the zeroth and second orders. To determine C_1, the first order Eqs. (1) to (3) must be used. Choosing $[A_1(0), A_2(0), A_3(0)] = (\sqrt{I_{1i}}, \sqrt{I_{2i}}, \sqrt{I_{3i}})$, we find

$$C_1 = \frac{\sqrt{I_{1i}I_{2i}I_{3i}}}{\gamma_C} - \frac{B_C}{\gamma_C^2}. \quad (23)$$

The growth rate γ_C recovers the growth rate γ derived above when $I_{2i} = I_{3i} = I_{20} = I_{30} = 0$.

B. Quantum theory for the three-wave interaction

The quantum theory for three-wave interaction is formulated by the field-theoretical method, i.e., by quantizing the classical fields A_j as quantum operators $\hat{A}_j$ on the occupation number states. The resulting Hamiltonian for a homogeneous (spatially independent) quantum three-wave interaction with complex coupling constant g is [7,13–15]

$$\hat{H} = ig\hat{A}_1^\dagger \hat{A}_2 \hat{A}_3 - ig^* \hat{A}_1 \hat{A}_2^\dagger \hat{A}_3^\dagger, \quad (24)$$

where the $\hat{A}_j^\dagger$, $\hat{A}_j$ $(j = 1, 2, 3)$ are creation and annihilation operators, respectively, and $[\hat{A}_j, \hat{A}_l^\dagger] = \delta_{jl}$. This Hamiltonian acts on the space of occupation number states $|n_1, n_2, n_3\rangle$, and commutes with operators $\hat{s}_2 = \hat{n}_1 + \hat{n}_3$ and $\hat{s}_3 = \hat{n}_1 + \hat{n}_2$, where the $\hat{n}_j = \hat{A}_j^\dagger \hat{A}_j$ are standard number operators. The $\hat{s}_2$ and $\hat{s}_3$ operators are identical in form to the constants of motion found in the classical theory, Eqs. (6) and (7), so we will write their expectation values identically, i.e., $\langle \hat{s}_2 \rangle = s_2$ and $\langle \hat{s}_3 \rangle = s_3$.

Because $\hat{s}_2$ and $\hat{s}_3$ commute with $\hat{H}$, their eigenstates form an invariant subspace of dimension $d = s_2 + 1$ [14,15] with states

$$\Psi(t) = \sum_{i=0}^{s_2} \alpha_i(t)\psi_i, \quad (25)$$

where

$$\psi_i = |s_2 - i, s_3 - s_2 + i, i\rangle. \quad (26)$$

It is assumed that the eigenvalue $s_3 \geqslant s_2$, which accounts for the asymmetry in the above equation. Within this subspace, the Hamiltonian is represented as a square tridiagonal matrix with vanishing diagonal. Taking the coupling constant $g = -i$, the matrix is also symmetric, with elements

$$H_{ij} = \delta_{i,j+1} h_i + \delta_{i+1,j} h_j, \quad (27)$$

$$h_i = \sqrt{(s_2 - i)(s_3 - s_2 + 1 + i)(i + 1)}. \quad (28)$$

As will be shown below, the phase of the coupling constant will not affect the dynamics of observables. Also, we emphasize that this quantization procedure using the field-theoretical method maps the classical nonlinear Hamiltonian specified by Eq. (4) into a quantum (linear) Hamiltonian operator on a finite-dimensional Hilbert space of dimension $d = s_2 + 1$. The recent quantum three-wave interaction simulation by Shi *et al.* [14] on Rigetti Computing hardware had $d = 3$.

Returning to Eq. (24) with an arbitrary coupling coefficient g, the Heisenberg equations are

$$\begin{aligned} \partial_t \hat{A}_1 &= g\hat{A}_2 \hat{A}_3, \\ \partial_t \hat{A}_2 &= -g^* \hat{A}_1 \hat{A}_3^\dagger, \\ \partial_t \hat{A}_3 &= -g^* \hat{A}_1 \hat{A}_2^\dagger, \end{aligned} \quad (29)$$

which are identical in form to the amplitude equations of the classical case, Eqs. (1) to (3), with classical wave amplitudes replaced by operators. Also as with the classical case, we may combine these equations using the constants of motion to find decoupled second-order equations for the number operators $\hat{n}_j = \hat{A}_j^\dagger \hat{A}_j$,

$$\partial_\tau^2 \hat{n}_1 = 2\left[\hat{s}_2\hat{s}_3 + 3\hat{n}_1^2 - (2\hat{s}_2 + 2\hat{s}_3 + 1)\hat{n}_1\right], \quad (30)$$

$$\partial_\tau^2 \hat{n}_2 = 2\left[\hat{s}_3(1 + \hat{s}_2 - \hat{s}_3) - 3\hat{n}_2^2 + (4\hat{s}_3 - 2\hat{s}_2 - 1)\hat{n}_2\right], \quad (31)$$

$$\partial_\tau^2 \hat{n}_3 = 2\left[\hat{s}_2(1 + \hat{s}_3 - \hat{s}_2) - 3\hat{n}_3^2 + (4\hat{s}_2 - 2\hat{s}_3 - 1)\hat{n}_3\right], \quad (32)$$

where $\tau = t|g|$ and $\partial_\tau^2 \hat{n}_1 = -\partial_\tau^2 \hat{n}_2 = -\partial_\tau^2 \hat{n}_3$. Note that Eqs. (30) to (32) depend only on the magnitude of the coupling constant, which has been absorbed by the normalized time parameter. Next, to fairly compare the quantum and classical equations, we take the expectation of Eqs. (30) to (32),

$$\partial_\tau^2 \langle n_1 \rangle = 2\left(s_2 s_3 + 3\langle n_1^2 \rangle - (2s_2 + 2s_3 + 1)\langle n_1 \rangle\right), \quad (33)$$

$$\partial_\tau^2 \langle n_2 \rangle = 2\left[s_3(1 + s_2 - s_3) - 3\langle n_2^2 \rangle + (4s_3 - 2s_2 - 1)\langle n_2 \rangle\right], \quad (34)$$

$$\partial_\tau^2 \langle n_3 \rangle = 2\left[s_2(1 + s_3 - s_2) - 3\langle n_3^2 \rangle + (4s_2 - 2s_3 - 1)\langle n_3 \rangle\right]. \quad (35)$$

Directly comparing the classical Eqs. (8) to (10) with their quantum counterparts defined above, we see that, as with the classical case, the right-hand sides of Eqs. (30), (31), and (32) differ only by their signs. There are also significant differences. Each equation now includes additional factors of the number of photons $\langle n_j \rangle$ on the right-hand side of the equations, and the last two equations also include additional constant factors. More importantly, the quantum and

classical second-order equations differ in that the quantum equations are not closed equations for photon number $\langle n_j \rangle$. They also depend on the variance $\delta_j = \langle n_j^2 \rangle - \langle n_j \rangle^2$. As will be discussed in Sec. III, the variance cannot be zero for all times except in the trivial solution $\langle n_1 \rangle = \langle n_2 \rangle = \langle n_3 \rangle = 0$. Since the variance is nonzero, either a closure must be established for Eqs. (33) to (35) to be useful, or the full Schrödinger equation must be solved numerically.

III. QUANTUM THEORY FOR THE THREE-WAVE INSTABILITY

In this section, we find an approximate solution for $\langle n_1 \rangle(\tau)$ which corresponds to the exponential growth of the unstable classical solution as discussed in Sec. II. This first requires assuming an initial condition so as to determine the variance δ_j. With an expansion of the variance, we then linearize Eq. (33) and find the growth rate of the quantum instability. The unstable solutions according to the classical and quantum descriptions of the three-wave interaction are compared. Finally, the approximate solution is validated by the numerical solution of the Schrödinger equation.

A. Approximate solution of the variance

We seek to solve Eq. (33), which depends on the variance δ_1. Estimating δ_1 requires considering the Schrödinger equation

$$i\partial_\tau \Psi = H\Psi, \tag{36}$$

where the Hamiltonian H is defined in Eq. (24) and the constant $\hbar = 1$. The Hamiltonian for the invariant subspace of constant s_2 and s_3 is a $d \times d$ matrix,

$$H = \begin{pmatrix} 0 & h_0 & 0 & 0 & 0 & \dots \\ h_0 & 0 & h_1 & 0 & 0 & \dots \\ 0 & h_1 & 0 & h_2 & 0 & \dots \\ 0 & 0 & h_2 & 0 & h_3 & \dots \\ \vdots & \vdots & \vdots & \vdots & \vdots & \ddots \end{pmatrix}, \tag{37}$$

where h_j are defined by Eq. (24). Equation (36) is a system of d coupled first-order differential equations

$$i\dot{\alpha}_0 = h_0\alpha_1, \tag{38}$$

$$i\dot{\alpha}_1 = h_0\alpha_0 + h_1\alpha_2, \tag{39}$$

$$\dots$$

$$i\dot{\alpha}_i = h_{i-1}\alpha_{i-1} + h_i\alpha_{i+1}, \tag{40}$$

which are written explicitly in terms of the basis vectors ψ_i defined in Eqs. (25) and (26). As basis vectors in this d-dimensional space, ψ_i can be represented as

$$\psi_i = (\underbrace{0, 0, \dots 0}_{i}, 1, 0, 0, \dots 0). \tag{41}$$

As a footnote, we point out that it is straightforward to show by construction that there exists a unique nontrivial equilibrium solution such that $\dot{\alpha}_i = 0$ for all i. However, this zero-energy eigenstate should not be viewed as the quantum counterpart of the equilibrium in the classical theory.

The variance of the observable $\hat{n}_1$ is

$$\begin{aligned} \delta &= \langle n_1^2 \rangle - \langle n_1 \rangle^2 \\ &= \sum_{j=0}^{s_2} |\alpha_j|^2 (s_2 - j)^2 - \left(\sum_{j=0}^{s_2} |\alpha_j|^2 (s_2 - j) \right)^2. \end{aligned} \tag{42}$$

Note that, for an infinitely narrow initial condition, where $\alpha_m(0) = 1$ and $\alpha_{i\neq m}(0) = 0$ for some m, the variance is zero. Using the above expression of δ_1, it can also be proven that its maximum value is $s_2^2/4$.

For a sufficiently narrow distribution of initial states, it may be possible to approximate the variance as a constant, so long as it does not grow too quickly in time. To justify this approximation, consider a narrowly distributed initial condition

$$\begin{aligned} \Psi(0) &= [\alpha_0(0), \alpha_1(0), \dots, \alpha_{s_2}(0)] \\ &= (\dots, \phi\varepsilon^2, \phi\varepsilon, \phi, \phi\varepsilon, \phi\varepsilon^2, \dots), \end{aligned} \tag{43}$$

where ϕ is a normalization such that $\sum_{i=0}^{s_2} |\alpha_i(0)|^2 = 1$ and $\varepsilon \ll 1$ is a small parameter describing how spread out the initial state is. Algebraically, this requires that, for some m, $\alpha_i(0) = \varepsilon^{|m-i|}\alpha_m(0)$, i.e., the initial distribution is centered around the mth state $|n_1, n_2, n_3\rangle = |s_2 - m, s_3 - s_2 + m, m\rangle$. At $\tau = 0$, the variance of $\hat{n}_1$ according to Eq. (42) is

$$\delta_1(\tau = 0) = \frac{2\varepsilon^2(1-\varepsilon^2)}{(1+\varepsilon^2)^2} \sum_{n=0}^{\infty} \varepsilon^{2n}[2n(n+1)+1]. \tag{44}$$

Then, assuming the time τ and spreading parameter ε are small, we may expand Eqs. (38) to (40) in terms of these small parameters to find the variance δ_1 as a series in orders of ε and τ. To first order in τ, δ_1 is also first order in ε,

$$\delta_1(\tau) = \delta_1(\tau = 0) + 2\varepsilon\tau(h_m - h_{m-1}) + O(\tau^2) + O(\varepsilon^2). \tag{45}$$

Note that it happens that each order in τ introduces a factor of a constant $h_i \sim h_m$, so we require that $\tau \ll 1/h_m$ for the expansion to hold. Thus, the growth of the variance δ_1 is linearly proportional to the small spreading parameter ε at short times, and we may provisionally take $\delta_1(\tau) = \delta_1(0)$, relying on the smallness of ε. We will check this assumption numerically below.

B. Quantum three-wave instability

We now proceed to solve Eq. (33) for a narrowly distributed initial condition described in Eq. (43). Denote by $(\langle n_1 \rangle, \langle n_2 \rangle, \langle n_3 \rangle) = (n_{1i}, n_{2i}, n_{3i})$, the initial expected occupation numbers. Letting $\langle n_1 \rangle = n_{1i} + \delta n_1$, and Taylor-expanding Eq. (33) around n_{1i}, we have

$$\begin{aligned} \delta\ddot{n}_1 = 2[&3\delta_1(\tau) + n_{2i}n_{3i} - n_{1i}(1 + n_{2i} + n_{3i}) \\ &+ \delta n_1(2n_{1i} - 2n_{2i} - 2n_{3i} - 1 + 3\delta n_1)]. \end{aligned} \tag{46}$$

Collecting terms allows us to define

$$\gamma_Q = 2\sqrt{n_{1i} - n_{2i} - n_{3i} - 1/2}, \tag{47}$$

and

$$B_Q(\tau) = 2n_{1i}(1 + n_{2i} + n_{3i}) - 2n_{2i}n_{3i} - 6\delta_1(\tau), \tag{48}$$

similarly to the classical definitions of γ_C and B_C, Eqs. (21) and (22). Thus, Eq. (46) can be written as

$$\delta\ddot{n}_1 = \delta n_1\left(\gamma_Q^2 + 6\delta n_1\right) - B_Q(\tau). \tag{49}$$

As in the classical case, when $\tau \ll 1/\gamma_Q$ (or equivalently $\delta n_1 \ll \gamma_Q^2$), the quadratic term may be neglected. Since the growth of δ_1 may be made arbitrarily small with ϵ, let us assume a constant variance such that $B_Q(\tau) = B_Q(0) \equiv B_Q$. This results in an approximate quantum three-wave interaction equation

$$\delta\ddot{n}_1 = \delta n_1\gamma_Q^2 - B_Q, \tag{50}$$

which is identical in form to the classical equation, Eq. (19), and also shares a solution of the same form

$$\delta n_1 = \frac{B_Q}{\gamma_Q^2} + C_1 e^{\gamma_Q\tau} + \left(\frac{B_Q}{\gamma_Q^2} + C_1\right)e^{-\gamma_Q\tau}, \tag{51}$$

where C_1 is a constant determined by the initial conditions. The above equation for δn_1 implies that the condition for instability in the quantum theory of the three-wave interaction (assuming an initial variance which grows slowly in time) is similar to the classical instability criterion, namely, that $\gamma_Q^2 > 0$.

Since it is not possible to formulate a first-order equation for $\langle n_1\rangle$ in lieu of the second-order Eqs. (30) to (32), the constant C_1 must be calculated directly from the Schrödinger equation at $\tau = 0$. Explicitly,

$$\delta\dot{n}_1(0) = \partial_\tau\langle n_1\rangle(0) = \sum_{i=0}^{s_2} 2\alpha_i(0)\dot{\alpha}_i(0)(s_2 - i), \tag{52}$$

where the time derivatives of the weights $\dot{\alpha}_i$ are given by Eqs. (38) to (40).

C. Classical correspondence

In summary, we found that the quantum theory for the three-wave interaction supports a quantum instability according to our definition of exponential growth of an observable from an initial condition. This quantum instability corresponds to the classical description of the instability, and the unstable solutions are structurally identical. Both require that the growth rate γ is real for an instability, and both are only applicable so long as the quadratic terms δI_1^2 and δn_1^2 are small. The growth rates

$$\gamma_Q = 2\sqrt{n_{1i} - n_{2i} - n_{3i} - 1/2},$$
$$\gamma_C = 2\sqrt{I_{1i} - I_{2i} - I_{3i}},$$

and other constants of the unstable solutions

$$B_Q = 2n_{1i}(1 + n_{2i} + n_{3i}) - 2n_{2i}n_{3i} - 6\delta_1(0),$$
$$B_C = 2I_{1i}(I_{2i} + I_{3i}) - 2I_{2i}I_{3i},$$

differ only by constant factors and the relative differences between these constants tend towards zero in the classical limit as $n_{1i}, n_{2i}, n_{3i} \to \infty$. Further, for a fixed spreading parameter $\varepsilon < 1$, the initial condition described in Eq. (43) will yield a variance that approaches zero in the classical limit.

There are crucial differences between the quantum and classical systems which do not diminish as the photon number increases though. First, the quantum wave action equation, Eq. (33), depends on the variance of the action, a purely quantum phenomenon. Although the effect of the variance on the approximate quantum solution may be reduced if the initial variance is chosen to be small, it still introduces a new independent parameter, which must be chosen carefully to result in instability. Second, the quantum system does not admit closed first-order equations for the wave amplitude as the classical system does in Eq. (5). This has the effect of making the constant C_1 in Eq. (51) nontrivial to calculate in the quantum system, and since C_1 depends on the initial variance, it will not, in general, converge to the classical value in the classical limit. Finally, the quantum theory does not have a zero-energy eigenstate corresponding to the classical equilibrium. The classical and quantum solutions being compared are the result of linearizations about an arbitrary initial condition instead of an equilibrium.

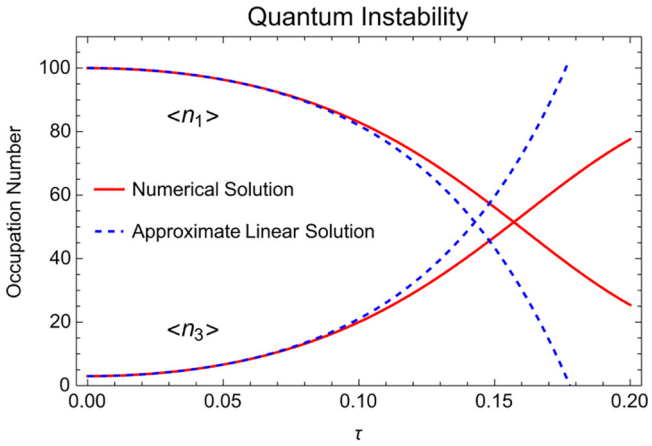

FIG. 1. Numerical solution of the Schrödinger equation, Eq. (36), and approximate linear solution, Eq. (51), of quantum system with the unstable initial condition $(n_{1i}, n_{2i}, n_{3i}) = (100, 10, 3)$. The spreading parameter is $\varepsilon = 0.1$, which yields $\delta_1(0) = 0.02$ and $C_1 = -3.9$.

D. Numerical solution of the quantum instability

In this subsection, we compare the approximate solution of quantum instability obtained with the numerical solution of the Schrödinger equation. For a fixed s_2 and s_3, we expect the quantum instability to have the highest growth rate when $(\langle n_1\rangle(0), \langle n_2\rangle(0), \langle n_3\rangle(0) \equiv (n_{1i}, n_{2i}, n_{3i}) = (s_2, 0, 0)$ and $s_2 = s_3$. This follows from the definition of the growth rate of the instability γ_Q in Eq. (47). Indeed, in the next section, this case will be used as an example to compare with stable initial conditions. For evaluating the validity of the approximate solution of quantum instability, Eq. (51), this system is also favorable because its initial variance δ_1 and spreading parameter ε are zero.

Here, we consider a less favorable unstable initial condition $(n_{1i}, n_{2i}, n_{3i}, \varepsilon) = (100, 10, 3, 0.1)$. Plotted in Fig. 1 are the exact quantum solutions to the Schrödinger equation and the approximate solution of Eq. (51) for that initial condition. Note that, while the derivation of the solution to the linearized Eq. (50) is only valid until $\tau \sim 1/h_{z_0} = 0.02$ as required by our expansion of the variance in Eq. (45), the linearized

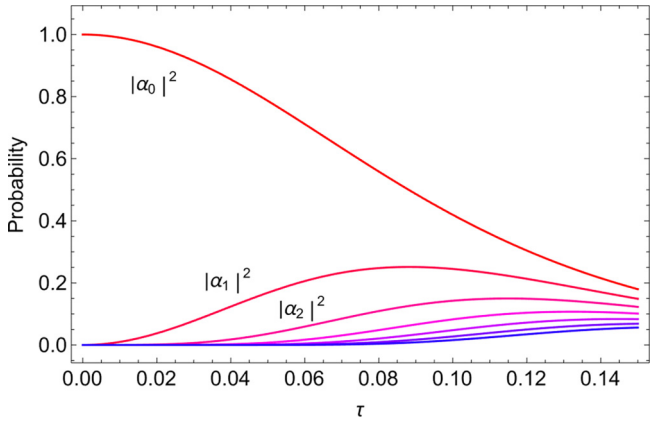

FIG. 2. Evolution of the probability of occupation number states for unstable initial condition $(n_{1i}, n_{2i}, n_{3i}) = (100, 0, 0)$ and spreading parameter $\varepsilon = 0$. This corresponds to $\alpha_0 = 1$ and $\Psi = \psi_0$ at $\tau = 0$. The first three states' probabilities are labeled and the first seven states are plotted.

solution matches the exact solution well beyond that point. At $\tau \sim 0.14$, the condition for the linearization $\delta n_1 \ll \gamma_Q^2$ breaks as $\delta n_1 \cong 50$ and $\gamma_Q^2 = 346$, and the approximate solution and exact solutions diverge. In the case of $(n_{1i}, n_{2i}, n_{i0}, \varepsilon) = (100, 0, 0, 0)$, the approximate solution remains valid much longer since the growth of the variance δ_1 is now second order in τ as shown in Eq. (45), and the initial condition imposes $\langle \dot{n}_1 \rangle(0) = 0$, keeping δn_1 smaller than γ_Q^2 for much longer.

IV. PROPERTIES OF THE QUANTUM THREE-WAVE INSTABILITY

In this section, we investigate the properties of the quantum instability through numerical solutions. It is demonstrated that the quantum instability is realized as a cascade of wave functions in the space of occupation number states. We also show that an instability-admitting Hamiltonian has a much richer spectrum than a stable Hamiltonian.

A. Quantum instability as a wave-function cascade in the space of occupation number states

The exponential growth in the occupation numbers shown in Eq. (51) and Fig. 1 is realized through a cascade of wave functions from states with higher $|n_1\rangle$ to states with lower $|n_1\rangle$. This cascade is particularly evident with an initial state which is maximally localized and also maximal in the expectation value of $\hat{n}_1$. Shown in Fig. 2 is such a probability cascade with initial condition $(n_{1i}, n_{2i}, n_{3i}) = (100, 0, 0)$, which initializes the $\psi_0 = |100, 0, 0\rangle$ state with a probability 1, i.e., $\alpha_0 = 1$ at $\tau = 0$.

Only the first seven states' probability evolution is shown in Fig. 2, but the cascade occurs through all 101 available states as shown in Fig. 3(a). The cascading behavior is characteristic of the instability in the three-wave interaction. In a stable system, with an otherwise identical initial probability distribution among its 101 states, the cascade does not occur as illustrated in Fig. 3(b) for the case of $(n_{1i}, n_{2i}, n_{3i}) = (100, 900, 0)$. It is interesting to note that the cascading process evident in Fig. 3(a) is maintained well past the time when the numerical solution and the approximate linear solution diverge. Also of note in Figs. 3(a) and 3(b) is the irreversibility of the unstable quantum system versus the guaranteed reversibility of the stable quantum system. The recurrence time shown in Fig. 3(b) is approximately $t = 0.1$.

We can further examine the state spreading in Fig. 3 via two kinds of correlators. The first is the two-point correlator $\langle V(0)V(t)\rangle$, where $V(t)$ is a Heisenberg operator and $\langle \dots \rangle$ represents a thermal average defined by

$$\langle X \rangle = \frac{1}{\mathrm{tr}(e^{-H/T})} \mathrm{tr}(e^{-H/T} X).$$

Here, tr() is the trace, T is the system temperature, H is the Hamiltonian, and X is a local, Hermitian unitary operator. The time it takes this correlator to decay is the dissipation time of the system [41,42]. We will consider local unitary operators which flip the probability of adjacent sites. That is, we define the operator $V(t) = X_i$ to be the identity except at sites ψ_i and ψ_{i+1} where X_i acts as the Pauli matrix σ_x, i.e., $X_i \Psi = X_i(\dots, \alpha_{i-1}, \alpha_i, \alpha_{i+1}, \alpha_{i+1}, \dots) = (\dots, \alpha_{i-1}, \alpha_{i+1}, \alpha_i, \alpha_{i+1}, \dots)$. With this definition, for a system

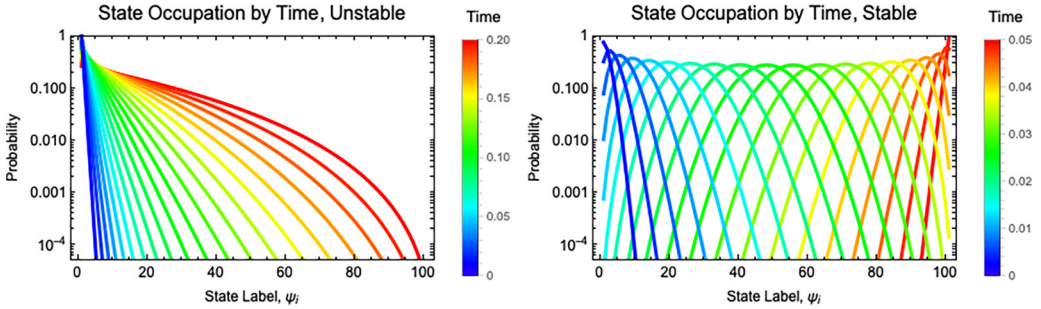

(a) (b)

FIG. 3. Probability distribution over occupation number states at various times, represented by different colors, for initial condition $\alpha_0^2(0) = 1$. For the unstable case (a), $s_2 = s_3 = 100$, while for the stable case (b), $s_2 = 100$ and $s_3 = 1000$. The unstable initial condition results in a cascade of probability among all 101 states and the variance monotonically increases. For the stable case, the variance oscillates with a recurrence time of approximately 0.1. Only the first half of the recurrence time is plotted in (b) for clarity. The unshown second half would overlap with the first half. (a) $(n_{1i}, n_{2i}, n_{3i}) = (100, 0, 0)$. (b) $(n_{1i}, n_{2i}, n_{3i}) = (100, 900, 0)$.

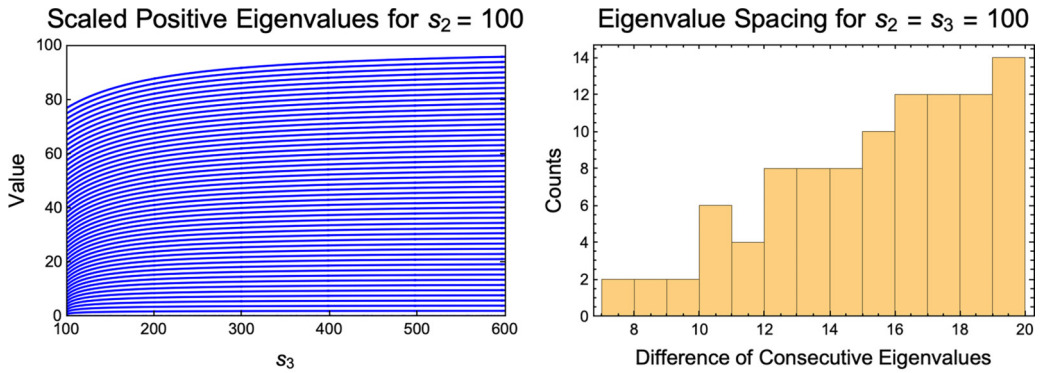

(a) (b)

FIG. 4. Eigenvalues of the $d = 101$ Hamiltonian with $s_2 = 100$. In (a) the positive eigenvalues are shown with s_3 varying from 100 to 600. The negative eigenvalues have the same magnitude as the positive ones. The eigenvalues approach constant spacing as $s_3 \to \infty$. In (b) the spacings between the eigenvalues are plotted as a histogram, corresponding to the leftmost portion of (a). As s_3 increases, the range of the histogram narrows. (a) Positive eigenvalues for $s_2 = 100$, scaled by $1/\sqrt{s_3}$. (b) Histogram of the differences between consecutive eigenvalues for $s_2 = s_3 = 100$.

with $s_2 = s_3 = 100$, the two-point correlator for X_0 decays halfway to its minimum value after $t \simeq .09$ for $T \gg 1$. This corresponds nicely with the time it takes the wave function to spread to roughly half of all available states in Fig. 3(a). The second correlator we will consider is an out-of-time-order correlator (OTOC), defined by

$$C(t) = -\langle [W(t), V(t=0)]^2 \rangle,$$

where $W(t)$, $V(t)$, and the thermal average have the same definitions as above. We find that for the unstable system ($s_2 = s_3 = 100$) this correlator grows exponentially, which much research associated with a transition to chaos. However, recent work showed that this need not be the case [26]. Indeed, other integrable quantum systems near unstable fixed points were also found to exhibit an exponential growth of $C(t)$ [22–25], leading us to characterize the state spreading evident in Fig. 3(a) as quantum scrambling rather than chaos [43].

The OTOC $C(t)$ can also be used to determine the time it takes for a measurement of V at $t = 0$ to have the maximal affect on a later measurement of W at t. With the same definitions of W and V, we find that it takes $t \simeq 0.3$ for $C(t)$ to reach a maximum in the unstable case is and $t \simeq 0.05$ in the stable case. This is half of the recurrence time for the stable case, as can be seen in Fig. 3(b).

B. Spectral properties of the instability

In this subsection, we will look closely at the eigenvectors and eigenvalues of the two $d = 101$ systems shown in Fig. 3, with $(s_2, s_3) = (100, 100)$ and $(s_2, s_3) = (100, 1000)$, respectively. The first system admits quantum instability and the second does not. According to the theoretical analysis developed in Sec. III, this is because, for the second system, $\gamma_Q^2/4 = \langle n_1 \rangle - \langle n_2 \rangle - \langle n_3 \rangle - 1/2 = 3\langle n_1 \rangle - s_3 - s_2 - 1/2 = 3\langle n_1 \rangle - 999.5 < 0$ since $\langle n_1 \rangle = s_2 - \langle n_3 \rangle < s_2$. The 50 positive eigenvalues for $s_2 = 100$, $s_3 \in [100, 600]$ are shown in Fig. 4(a). The negative eigenvalues are reflections of the positive ones. For the stable system, the eigenvalues are linearly distributed to a high precision, i.e.,

$$\begin{aligned}
\lambda_0 &\approx 50\lambda_{49}, \\
\lambda_1 &\approx 49\lambda_{49}, \\
&\vdots \\
\lambda_{49} &\approx -2\sqrt{s_3}, \\
\lambda_{50} &= 0, \\
\lambda_{51} &\approx -\lambda_{49}, \\
&\vdots \\
\lambda_{100} &\approx -50\lambda_{49},
\end{aligned} \tag{53}$$

while it can be seen in Fig. 4(a) that the eigenvalues in the unstable case are nonlinearly distributed. For intermediate values of $s_3 > s_2$ and $s_3 < 1000$, the eigenvalues slowly transition from a nonlinear to a linear distribution. Figure 4(b) shows the distribution of eigenvalue spacings for the unstable system, corresponding to the left-hand side of Fig. 4(a). As s_3 increases, the range of the distribution narrows and the separation between the eigenvalues approaches a constant value. For the case shown, with $s_2 = s_3 = 100$, the distribution of eigenvalue spacing appears approximately linear, with the difference between most consecutive eigenvalues being relatively large. This is in strong contrast to the distribution of eigenvalue spacings found in random matrix theory, in which, if the matrix elements are chosen from a Gaussian distribution (with the condition that the matrix be Hermitian), we would expect a Wigner distribution.

The linearity of the eigenvalues for the stable case places strong limitations on the allowable dynamics of the system. To see this directly, we analyze the frequency decomposition of the expectation of the occupation numbers. Denote by $\mathbf{v}_j$ the eigenvectors of H. In the ψ_j bases

$$\mathbf{v}_j = \sum_{k=0}^{s_2} \beta_{jk} \psi_k, \tag{54}$$

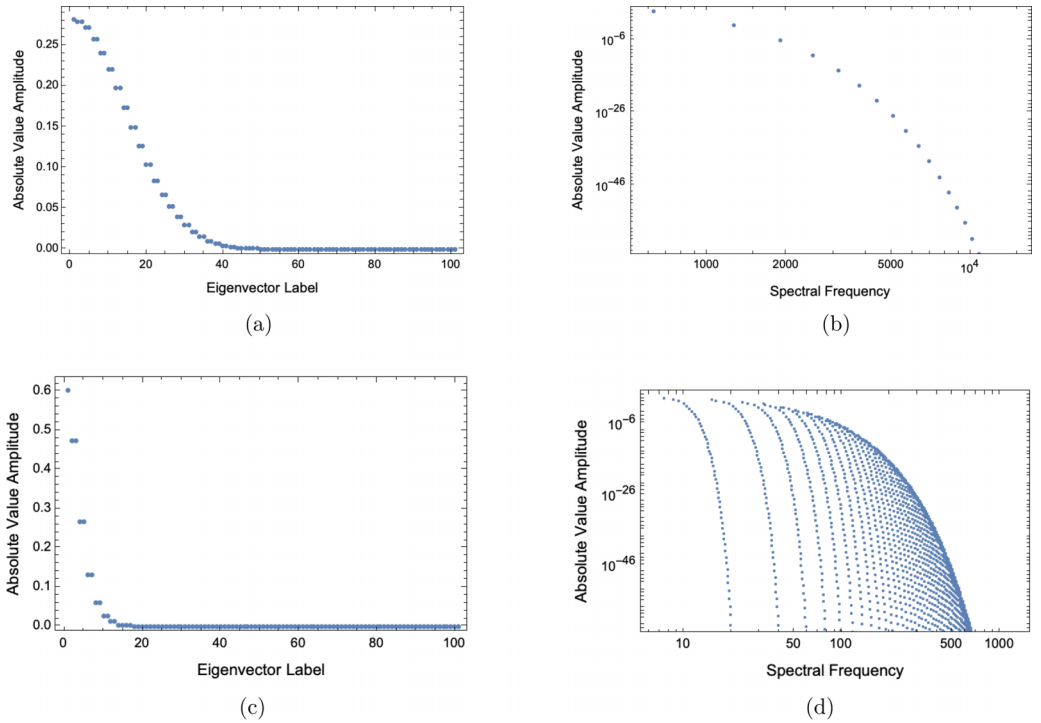

FIG. 5. Eigenvector weights ϵ_i and spectrum weight of of $\langle n_3\rangle(t)$ (the coefficients $\epsilon_i\epsilon_j\beta_{ik}\beta_{jk}$ for each frequency $\lambda_i-\lambda_j$ in Eq. (59)) for the stable $(s_2, s_3) = (100, 1000)$ and unstable $(s_2, s_3) = (100, 100)$ systems. The initial condition is $\alpha_0 = 1$, which corresponds to the $\psi_0 = |100, 0, 0\rangle$ mode having probability 1. Most of the 101 and 2551 spectral modes have zero amplitude in (b) and (d), respectively, and are not displayed. (a) Amplitude of eigenvectors, ϵ_i, of the stable system. (b) Spectrum weight of $\langle n_3\rangle(t)$ for the stable system. (c) Amplitude of eigenvectors, ϵ_i, of the unstable system. (d) Spectrum weight of $\langle n_3\rangle(t)$ for the unstable system.

which defines the transformation matrix β_{jk}. For a state $\Psi(t)$, we have

$$\Psi(t) = \sum_{j=0}^{s_2} \alpha_j(t)\psi_j = \sum_{j=0}^{s_2} \epsilon_j \mathbf{v}_j e^{-i\lambda_j t}. \tag{55}$$

This then identifies

$$\alpha_j(t) = \sum_{k=0}^{s_2} \epsilon_k \beta_{kj} e^{-i\lambda_k t}. \tag{56}$$

The expectation $\langle n_3\rangle(t)$ can be evaluated as

$$\langle n_3\rangle = \sum_{j=0}^{s_2} |\alpha_j(t)|^2 j \tag{57}$$

$$= \sum_{j=0}^{s_2} \left| \sum_{k=0}^{s_2} \epsilon_k \beta_{kj} e^{-i\lambda_k t} \right|^2 j \tag{58}$$

$$= \sum_{j=0}^{s_2}\sum_{k=0}^{s_2} |\epsilon_k\beta_{kj}|^2 j + \sum_{j=0}^{s_2}\left\{\sum_{k=1}^{s_2}[\epsilon_0\epsilon_k\beta_{0j}^\dagger\beta_{kj}e^{i(\lambda_0-\lambda_k)t} + \text{c.c.}] + \sum_{k=2}^{s_2}[\epsilon_1\epsilon_k\beta_{1j}^\dagger\beta_{kj}e^{i(\lambda_1-\lambda_k)t} + \text{c.c.}] + \ldots + \epsilon_{s_2-1}\epsilon_{s_2}\beta_{s_2-1,j}^\dagger\beta_{s_2 j}e^{i(\lambda_{s_2-1}-\lambda_{s_2})t} + \text{c.c.}\right\}. \tag{59}$$

The spectral frequencies available for $\langle n_3\rangle(t)$ are the differences between each pair of the eigenfrequencies $\lambda_i - \lambda_j$ where $i \neq j$. The weights are determined by the weighting of eigenvectors ϵ_i and the transformation matrix β_{kj}.

For the stable quantum Hamiltonian with $(s_2, s_3) = (100, 1000)$ defined above, the linear spacing of its eigenvalues means that there are only 101 spectral frequencies (corresponding to combinations of the 50 distinct eigenvalue absolute values and the 0 eigenvalue) available for $\langle n_3\rangle(t)$. It also implies that its spectrum constitutes a Fourier series. By contrast, the unstable Hamiltonian with $(s_2, s_3) = (100, 100)$ has $\text{Floor}(d^2/4) + 1 = 2551$ spectral frequencies available. The values of the spectral frequencies, not just their quantity, are also important. The maximum recurrence time, when the system will begin to repeat itself, in either system will be the least common multiple of the spectral periods. For the stable Hamiltonian, this value is guaranteed to exist since the Fourier periods will all be rational multiples of a single, base period. Conversely, in the unstable system, only Poincaré recurrence, not exact recurrence, is possible. This irreversibility is a familiar hallmark of instability in a classical system.

The amplitude of eigenvalues and frequency spectrum of the stable and unstable systems given the initial

condition $\alpha_0(0) = 1$ are plotted in Fig. 5. The unstable system is $(s_2, s_3) = (100, 100)$ with $(n_{1i}, n_{2i}, n_{3i}) = (100, 0, 0)$ and the stable system is $(s_2, s_3) = (100, 1000)$ with $(n_{1i}, n_{2i}, n_{3i}) = (100, 900, 0)$. The spectral differences between the stable and unstable quantum systems discussed above are evident.

V. DISCUSSION AND CONCLUSION

The quantum theory of the three-wave interaction, obtained by quantizing the classical Hamiltonian using a field-theoretical method, maps the nonlinear classical Hamiltonian into a finite-dimensional Hermitian system. We showed that the quantum theory admits a quantum instability corresponding to the classical three-wave instability. The quantum and classical descriptions of the three-wave instability require the same conditions to occur, with the quantum theory having additional requirements on the variance of its initial condition. In the classical limit, both theories predict the same growth rate. We numerically demonstrated that this quantum instability is realized as a cascade of wave functions in the space of occupation number states, and further showed that such a cascade does not occur with a stable Hamiltonian. The Hamiltonian of an unstable quantum system is shown to possess a much richer spectrum than the Hamiltonian of a stable quantum system. Additionally, the unstable quantum system has a much longer recurrence time than the stable system.

Current technology allows for the quantum three-wave instability to be simulated using quantum hardware. The work performed by Shi *et al.* in simulating the quantum three-wave interaction utilized only two qubits and three of their four possible states, $|00\rangle$, $|01\rangle$, and $|10\rangle$, to represent $d = s_2 + 1 = 3$ states [14]. Although the linear solution given by Eq. (51) could have been simulated, the growth rate of the quantum instability would have been too small to notice at such a low dimension. Also, the dimension was too small to compare with the classical instability. However, since the number of states representable by n qubits is $d \propto 2^n$, quantum hardware with sufficient numbers of qubits to simulate the quantum instability and compare to the classical instability already exists [44]. Of course, this issue is complicated by the unitary operator needing $d^2 = 2^{n^2}$ gates to be approximated using the gates available to the system. Though the method of implementing a single, specially made gate as in Ref. [14] somewhat mitigates this problem.

ACKNOWLEDGMENT

This research was supported by the U.S. Department of Energy (Contract No. DE-AC02-09CH11466).

[1] J. Moody, P. Michel, L. Divol, R. Berger, E. Bond, D. Bradley, D. Callahan, E. Dewald, S. Dixit, M. Edwards *et al.*, Nat. Phys. **8**, 344 (2012).
[2] J. Myatt, J. Zhang, R. Short, A. Maximov, W. Seka, D. Froula, D. Edgell *et al.*, Phys. Plasmas **21**, 055501 (2014).
[3] V. Zakharov, V. L'vov, and G. Falkovich, *Kolmogorov Spectra of Turbulence I: Wave Turbulence* (Springer, New York, 2012).
[4] L. Frantz and J. Nodvik, J. Appl. Phys. **34**, 2346 (1963).
[5] J. Ahn, A. Efimov, R. Averitt, and A. Taylor, Opt. Express **11**, 2486 (2003).
[6] G. Brunton, G. Erbert, D. Browning, and E. Tse, Fusion Eng. Des. **87**, 1940 (2012).
[7] Y. Shi, Plasma physics in strong field regimes, Ph.D. thesis, Princeton University, 2018.
[8] M. Rosenbluth, R. White, and C. Liu, Phys. Rev. Lett. **31**, 1190 (1973).
[9] V. E. Zakharov and S. V. Manakov, Zh. Eksp. Teor. Fiz. **69**, 1654 (1975).
[10] D. J. Kaup, A. Reiman, and A. Bers, Rev. Mod. Phys. **51**, 275 (1979).
[11] A. Reiman, Rev. Mod. Phys. **51**, 311 (1979).
[12] K. Ohkuma and M. Wadati, J. Phys. Soc. Jpn. **53**, 2899 (1984).
[13] Y. Shi, H. Qin, and N. J. Fisch, Phys. Rev. E **96**, 023204 (2017).
[14] Y. Shi, A. R. Castelli, X. Wu, I. Joseph, V. Geyko, F. R. Graziani, S. B. Libby, J. B. Parker, Y. J. Rosen, L. A. Martinez, and J. L. DuBois, Phys. Rev. A **103**, 062608 (2021).
[15] Y. Shi, H. Qin, and N. J. Fisch, Phys. Plasmas **28**, 042104 (2021).
[16] F. Haake, *Quantum Signatures of Chaos*, 3rd ed. (Springer, New York, 2010).
[17] L. E. Reichl, *The Transition to Chaos*, 2nd ed. (Springer, New York, 2004).
[18] J. Bellissard, in *Schrödinger Operators*, Lecture Notes in Mathematics, Vol. 1159, edited by S. Graffi (Springer, Berlin, Heidelberg, 1985).
[19] B. V. Chirikov, Phys. Rep. **52**, 263 (1979).
[20] J. A. Armstrong, N. Bloembergen, J. Ducuing, and P. S. Pershan, Phys. Rev. **127**, 1918 (1962).
[21] J.-S. Caux and J. Mossel, J. Stat. Mech. (2011) P02023.
[22] S. Pappalardi, A. Russomanno, B. Žunkovič, F. Iemini, A. Silva, and R. Fazio, Phys. Rev. B **98**, 134303 (2018).
[23] Q. Hummel, B. Geiger, J. D. Urbina, and K. Richter, Phys. Rev. Lett. **123**, 160401 (2019).
[24] S. Pilatowsky-Cameo, J. Chávez-Carlos, M. A. Bastarrachea-Magnani, P. Stránský, S. Lerma-Hernández, L. F. Santos, and J. G. Hirsch, Phys. Rev. E **101**, 010202(R) (2020).
[25] B. Bhattacharjee, X. Cao, P. Nandy, and T. Pathak, J. High Energy Phys. 05 (2022) 174.
[26] W. Kirkby, D. H. J. O'Dell, and J. Mumford, Phys. Rev. A **104**, 043308 (2021).
[27] C. M. Bender and S. Boettcher, Phys. Rev. Lett. **80**, 5243 (1998).
[28] C. M. Bender, D. C. Brody, and H. F. Jones, Phys. Rev. Lett. **89**, 270401 (2002).

[29] C. M. Bender, Rep. Prog. Phys. **70**, 947 (2007).
[30] A. Mostafazadeh, J. Math. Phys. **43**, 205 (2002).
[31] H. Qin, R. Zhang, A. S. Glasser, and J. Xiao, Phys. Plasmas **26**, 032102 (2019).
[32] H. Qin, Y. Fu, A. S. Glasser, and A. Yahalom, Phys. Rev. E **104**, 015215 (2021).
[33] R. Zhang, H. Qin, and J. Xiao, J. Math. Phys. **61**, 012101 (2020).
[34] I. Dodin and E. Startsev, Phys. Plasmas **28**, 092101 (2021).
[35] K. Kustura, C. Gonzalez-Ballestero, A. de los Ríos Sommer, N. Meyer, R. Quidant, and O. Romero-Isart, Phys. Rev. Lett. **128**, 143601 (2022).
[36] K. Kustura, C. C. Rusconi, and O. Romero-Isart, Phys. Rev. A **99**, 022130 (2019).
[37] V. I. Kuvshinov, V. V. Marmysh, and V. A. Shaparau, Theor. Math. Phys. **139**, 846 (2004).
[38] R. Sagdeev and A. Galeev, *Nonlinear Plasma Theory* (W. A. Benjamin, New York, 1969).
[39] A. Jurkus and P. N. Robson, Saturation effects in a travelling-wave parametric amplifier, in *Proceedings of the IEEE-Part B: Electronic and Communication Engineering* (IEEE, New York, 1960), Vol. 107.
[40] E. T. Jaynes and F. W. Cummings, Comparison of quantum and semiclassical radiation theories with application to the beam maser, in *Proceedings of the IEEE* (IEEE, New York, 1963), Vol. 51.
[41] J. Maldacena, S. H. Shenker, and D. Stanford, J. High Energy Phys. 08 (2016) 106.
[42] K. Richter, J. D. Urbina, and S. Tomsovic, J. Phys. A: Math. Theor. **55**, 453001 (2022).
[43] T. Xu, T. Scaffidi, and X. Cao, Phys. Rev. Lett. **124**, 140602 (2020).
[44] https://www.rigetti.com/what-we-build.